AIAA JOURNAL
Vol. 49, No. 3, March 2011

Experimental and Numerical Study of Jets from Elliptic Nozzles with Conic Plug

David Munday,* Mihai Mihăescu,† and Ephraim Gutmark‡
University of Cincinnati, Cincinnati, Ohio 45221

DOI: 10.2514/1.J050587

The study presents results concerning jets exhausting from elliptic nozzles with conic centerbody plugs. A nozzle with 3:1 ratio of exit heights is surveyed experimentally using particle image velocimetry for jet Mach numbers from 0.24 to 1.0, heated and unheated. At the exit, the nozzle inner surface has a slope of zero in the major axis plane, while in the minor axis plane the slope is steeper than that for a corresponding round nozzle. The conic plug causes splitting of the initial elliptic jet into two jets with their centerlines in the major-axis plane of the elliptic nozzle. Increasing M_j or total temperature causes the bifurcated potential cores of the individual jets to be slightly smaller and to diverge from one to another at a slightly greater angle from the nozzle centerline. Large eddy simulations of the experimental nozzle and two alternate nozzles are analyzed to find how the flow features are influenced by not forcing the jet towards the conic plug in the minor axis plane and by changing the ratio of exit heights to 2:1. Changing nozzle shape caused reduction in the spreading rate in the major axis and increase in spreading in the minor axis. Bifurcation occurs for all nozzles studied.

Nomenclature

A	=	exit area
a	=	speed of sound
$c_{0.5}$	=	half width of bifurcated jet
D_{eq}	=	equivalent diameter, $2\sqrt{A/\pi}$
h_y	=	major axis exit height
h_z	=	minor axis exit height
M_j	=	jet Mach number
NPR	=	nozzle pressure ratio, p_0/p_a
p_a	=	ambient pressure outside the jet
p_0	=	total pressure
T_a	=	ambient temperature outside the jet
T_0	=	total temperature
U_c	=	velocity in center of bifurcated jet
U_j	=	ideal jet velocity (isentropic, quasi-one-dimensional)
$y_{0.5}$	=	half width in major axis
$z_{0.5}$	=	half width in minor axis

I. Introduction

TURBULENT jets comprise a class of flows of fundamental scientific and engineering interest with wide application to mixing, heat transfer, combustion, and acoustics. Many experimental and numerical investigations have been carried out to study the various characteristics of jet flows. Simple round jets have been extensively studied experimentally and analytical expressions for the centerline velocity decay in the self preserving region of the jet have been derived [1–4].

Presented as Paper 2008-0760 at the 46th AIAA Aerospace Sciences Meeting and Exhibit, Reno, NV, 7–10 January 2008, and as Paper 2009-0079 at the 47th AIAA Aerospace Sciences Meeting and Exhibit, Orlando, FL, 5 January 2009; received 1 April 2010; revision received 27 September 2010; accepted for publication 8 November 2010.

*Graduate Student, Aerospace Engineering Department, ML 0070. Member AIAA.

†Research Assistant Professor, Aerospace Engineering Department, ML 0070. Member AIAA.

‡Distinguished Professor; Ohio Regents Eminent Scholar, Aerospace Engineering Department, ML 0070. Fellow AIAA.

The characteristics of noncircular jets have been found to differ significantly from axisymmetric jets. Experimental measurements have shown that noncircular jets can develop such that their cross sections can evolve into shapes similar to that at the nozzle exit, but with the axes switched [5–11]. Other studies found conditions in which this axis switching will not occur [12,13] The evolution of elliptic jets is governed by the initial conditions at the nozzle exit. The specific conditions that must exist in the near-field region of a noncircular jet in order for the dynamics of vortex self induction to lead to axis switching have been identified [13]. The vortex ring dynamics responsible for the axis switching observed involve self induction that is strongest where the local ring radius of curvature is smallest. The local radius of curvature is smallest in an ellipse at the ends of the major radii so these ends convect faster than the ends of the minor radii leading to the distortion of the ring out of plane. For an aspect ratio of 2:1 the evolution of the rings is such that the bending of what was originally the minor axis causes the local radius of curvature to become smaller while what was originally the major axis sees an increase in local radius of curvature until the two axes reverse and the jet switches orientation. The three dimensional evolution of the vortex rings leads the jet to engulf and entrain surrounding fluid increasing entrainment by a factor of 8 relative to a circular jet [6]. Conditions upstream of a jet nozzle, such as those in which the cross-section of the inlet duct changes or in any case with tabs or chevrons will also include streamwise vortices which mutually induct one another. This has also been shown in some cases to drive axis switching [14].

Elliptic jets with higher aspect ratios have been observed to perform a single axis switch followed by vortex ring splitting (bifurcation of the jet) [8]. In these situations the ends of the vortical rings meet, cut and connect before a second axis switch can occur. Bifurcation has also been observed in axisymmetric jets with combined helical and symmetric forcing if the ratio of the forcing frequencies is near two [9].

Computational fluid dynamics has become an important tool in investigating turbulent flowfields. Both compressible and incompressible simulations have been performed on noncircular and round turbulent jets. A variety of approaches like Reynolds-averaged Navier–Stokes (RANS/unsteady RANS) [15], direct numerical simulation (DNS) [16–18], large eddy simulation (LES) [19–23], and detached eddy simulation [24] have been used. For the case of high Reynolds number flows of practical interest DNS is still a prohibitively expensive technique. RANS based models have difficulty treating highly anisotropic flows and cannot predict the flow dynamics particularly important when analyzing noncircular jets. In recent decades it has been shown that LES represents the most

realistic approach for predicting such flow situations. LES has been successfully used to capture the vortex ring bifurcation phenomena and to expose the vorticity geometries in the flowfield near the jet exit for several aspect ratios of rectangular jets [22,23].

The present work represents an experimental [particle image velocimetry (PIV)] and numerical (LES) research effort to study how the introduction of a centerbody changes the behavior of elliptic jets. Several important engineering problems like separate-flow exhaust nozzles from jet engines employ nozzles that include a plug, but most of the published work on jets is for nozzles with no plug or centerbody within their exit planes.

II. Methods and Case Formulation

Nozzle 1, sketched in Fig. 1, was used in the experiments, and simulated with LES. This nozzle was designed to study the effect of a centerbody on elliptic jet development including axis switching. The centerbody is typical of one used on a jet engine exhaust nozzle. The geometry of this elliptic nozzle has been chosen to have a nozzle annular height at the major axis three times that of the minor axis ($h_y = 3h_z$). The differences in exit heights forces a difference in the exit angle of the nozzle. Thus, the exit in the minor axis inclines 21.5° from the nozzle centerline while the exit in the major axis inclines only 3.5° from the centerline. By comparison, an axisymmetric nozzle with the same centerbody and having the same exit area has an exit angle of 12° all around the nozzle. The centerbody has a half-angle of 16° and extends $1.79D_{eq}$ beyond the exit plane of the nozzle. The flow from this nozzle was found to bifurcate for all conditions. The centerbody shown in Fig. 1 is attached to an upstream support which is cylindrical in shape and tangent at the mating surface. The upstream end of this support has a hemispheric surface. The centerbody support is fixed in place by four support pylons with low drag symmetrical airfoil sections. When PIV of the same centerbody was tested with a round nozzle the wakes of the four supports were indiscernible. The supply piping for the nozzle contains flow straightening and stilling screens. Velocities within the stilling chamber were measured for the cold jet case and found to be nearly constant across the radius of the stilling chamber. This section is followed by fifth-order-polynomial contraction which feeds the nozzles. Further details of the conditions upstream are available in [25].

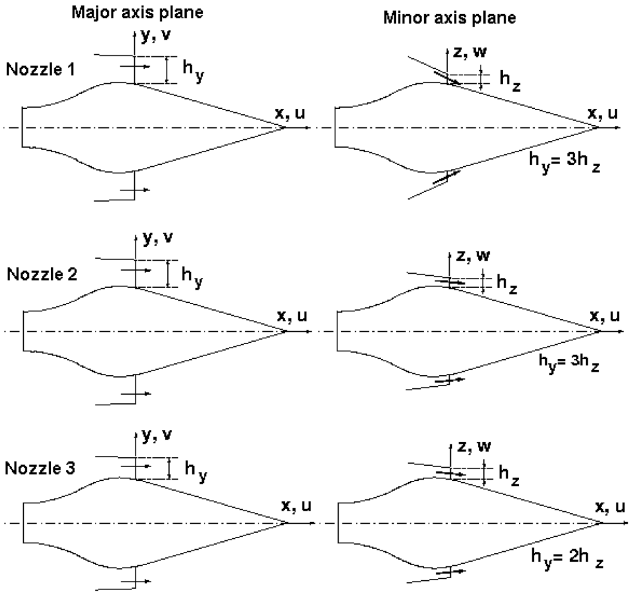

Fig. 1 Sketches of elliptical plug nozzle geometries and a picture of nozzle 1 mounted on the rig looking upstream.

To better understand this bifurcating behavior two additional geometries were simulated with LES. It was originally conjectured that the bifurcation might be caused by the significant inward radial velocity imposed in the minor axis by the contour of the nozzle inner surface which is steeper that it would be for a corresponding round nozzle (i.e. 21.5° for the elliptic nozzle as opposed to 12°). To explore this idea a LES case was set up with the nozzle having the same exit area, but with the negative radial component of velocity reduced so that the flow in the minor axis plane emerges parallel to the centerbody surface at a 16° angle with reference to the centerline of the nozzle. This case was named as nozzle 2 and the sketch of the nozzle is shown in Fig. 1.

To examine the possibility that the bifurcation was caused by excessive aspect ratio a third case was constructed. Nozzle 3 was designed to have an exit radial velocity profile similar to nozzle 2, but to have an aspect ratio of 2:1 ($h_y = 2h_z$). As in the case of nozzle 2 configuration, the flow in the minor axis plane emerges parallel to the centerbody surface at an angle of 16° while the flow in the major axis plane emerges almost parallel with the centerline of the nozzle at an angle of only 3.5° from the centerline. A sketch for nozzle 3 is also depicted in Fig. 1.

Experimentally, nozzle 1 was operated cold ($T_0/T_a = 1.0$) and hot ($T_0/T_a = 1.26$) with nozzle pressure ratios (NPRs) from 1.04 up to 1.89, giving jet Mach numbers, M_j of 0.24 to 1.0. These cases were measured using PIV. Reynolds numbers based on equivalent diameter range from 0.21 million to 1.05 million. LES was run on all three nozzles to calculate the turbulent flow associated with the hot jet case at the NPR of 1.8 giving an M_j of 0.96. Comparisons have been made between the experiments and the LES results for nozzle 1 case. Both experimental and numerical methodologies are described in the present section.

A. Experimental Facility and Procedure

The Gas Dynamics and Propulsion Laboratory at the University of Cincinnati has a scale model of a separate-flow jet engine exhaust system. For the present experiment a new elliptic nozzle has been designed and manufactured to mate with this existing and proven apparatus. This model is fed from a compressed air supply and the incoming air can be heated through a steam-to-air heat exchanger. The secondary flow nozzle is used only to supply seed for the PIV system. The secondary flow Mach number is in all cases negligible.

The principal tool used in the experimental investigation is a LaVision Stereoscopic PIV system. This instrument has been employed on the jet model previously and has proven effective at capturing three-component velocity measurements in any number of cross-stream planes. By measuring an entire plane simultaneously one eliminates one source of measurement error; when using constant temperature anemometry or pitot measurements the set-point of the jet will inevitably drift slightly while the probe is

scanning the entire flowfield point by point. This superimposes "tunnel drift" on top of the actual spatial variation in velocity field under study. By making a single-shot simultaneous planar measurement, this drift is eliminated for an entire cross cut.

The PIV system is set up with the laser casting a light sheet in a plane normal to the nozzle axis. Two laser pulses are generated separated by 2 μs. Two cameras are mounted outside the jet and tilted toward the axis so that they each view the illuminated sheet from an angle 45° from the sheet normal. Schiempflug adapters were employed to bring illuminated plane into focus. Each camera then resolves two components of velocity normal to its own angle of view. The resulting four components (two from each camera) are then projected onto the three normal components of the jet's coordinate system. It is extremely unlikely that a spurious vector generated from one camera will be compatible with the corresponding vector from the other, so the four-to-three mapping serves as a filter to remove spurious vectors. The PIV system takes multiple pairs of images at a rate of five pairs per second. Five hundred image pairs are taken in every case except $M_j = 1.00$, $T_0/T_a = 1.00$ for which 200 pairs were taken. The pixel size was 80×80 μm. The maximum displacement was 6.2 pixels. Taking a conservative estimate of 0.1 pixels for the uncertainty in displacement measured gives 1.6% uncertainty. This amounts to 5.6 m/s. The data was processed with an iterative procedure beginning with an integration window size of 64×64 pixels and refining this down to 4×4 pixels with a 50% overlap.

The entire PIV suite, laser and both cameras are mounted on a traverse which allows the system to be translated, undisturbed, to any streamwise location allowing many cross cuts to be measured without the loss of time in changing setups and without the uncertainties which come from repeated adjustment of components.

B. Numerical Procedure

The unsteady LES numerical flow calculations were performed for all three nozzles considered under the hot jet condition ($T_0/T_a = 1.26$) at the NPR of 1.8 ($M_j = 0.96$). The non-dimensionalized flow governing equations, namely continuity, momentum, and energy equations are discretized on a Cartesian, staggered grid using finite-differences. High order finite-differences are used for the spatial discretization of the momentum equations, where the convective terms are discretized with a third order accurate upwind scheme [26] while the diffusive terms are discretized with a fourth-order central finite difference scheme. Second-order schemes are used for the spatial discretization of the energy equation. The integration in time of the momentum equations is done through a second-order implicit scheme. The coupling between the velocity field and the pressure field is strong, since an iterative pressure-correction method with simultaneous velocity and pressure update is employed. The temporal discretization of the energy equation is performed with an explicit, three-step, low-storage Runge–Kutta scheme. The numerical efficiency is enhanced by using local mesh refinements in regions with large gradients in flow variables and by solving the problem at each time step using a fast multigrid method. The blocked-cell approach is used to handle nozzle's geometry [27].

Turbulence is modeled based on the LES approach without the explicit modeling of the subgrid scale (SGS) terms. Instead, the dissipation of the numerical scheme accounts for the SGS dissipation at the level of the smallest turbulent scales. Using the present approach, it has been shown that one may use different SGS models (such as the germano like dynamic, differential dynamic, or scale similarity) with the general result that the most important factor is grid resolution rather than the specific SGS model. Comparisons between the results obtained with and without explicit (different) SGS terms have shown that, for sufficiently fine grid resolution, the SGS terms may be neglected [28]. The grid resolution effect on the numerical solution has previously been addressed for a jet exhausting an axisymmetric coaxial nozzle with centerbody having the same core-stream exit area and similar conditions imposed for the core-stream jet as are used in this study [29]. Significant differences (above 10%) were observed between the results obtained on the coarsest grid and the results computed on the two finer ones. The results obtained with the intermediate grid and with the finest one were close to each other, suggesting that grid convergence had been achieved. The finest Cartesian grid used in the grid sensitivity study [29] is employed here to discretize the computational domain. The presented methodology has been successfully applied in past for studying turbulent flows [20,30,31].

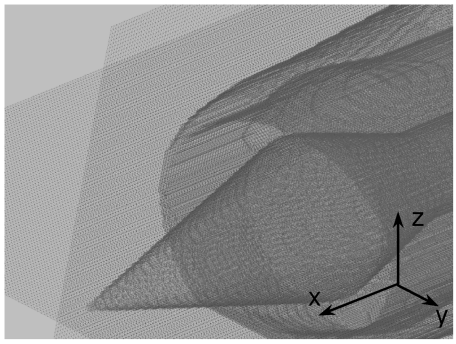

Fig. 2 Lateral view of the computational grid describing the elliptic nozzle with centerbody (nozzle 1).

Details of the computational Cartesian grid generated around of the 3:1 elliptic nozzle (nozzle 1) are presented in Fig. 2. The computational domain (about 6×10^6 computational cells, with local mesh refinements) has a square cross-section of roughly $15D_{\text{eq}} \times 15D_{\text{eq}}$ and a length of $30D_{\text{eq}}$. In the present computations the inlet, outlet and wall boundary conditions are used for solving the flowfield. Additionally, initial conditions must be specified at the beginning of the computations. Inlet boundary conditions were constant values for the flow velocity and temperature. At the solid surfaces, no-slip boundary conditions for the velocity and constant value for temperature are set. A flux conserving, zero-gradient boundary condition is applied at the outlet of the computational domain. The LES results were statistically averaged for a period of 30,000 time steps corresponding to approximately 15 flow-through times, achieving a converged solution at each time step.

III. Results

Across the entire range of velocities and temperatures examined, the gross character of the flow is the same. In every case the main stream bifurcates into two jets. By the end of the centerbody tip the potential core splits completely and the two potential regions generated diverge as the jet spreads. There are subtle differences in the core length and spreading rate depending on temperature and NPR, but the overall behavior is similar for all conditions considered.

A. PIV and LES Data Comparison

Figure 3 shows contours of normalized mean axial velocity as measured by PIV for nozzle 1, $M_j = 0.96$ and $T_0/T_a = 1.26$. The contours are in planes normal to the nozzle axis and located at $x/D_{\text{eq}} = 2.27$, $x/D_{\text{eq}} = 3.23$, and $x/D_{\text{eq}} = 4.19$ in the streamwise direction from the nozzle exit plane. The data are normalized by U_j, the ideal jet velocity at the exit. A corresponding three-dimensional visualization of the jet calculated by LES is presented in Fig. 4.

LES prediction and PIV measurement data are compared for this same case (nozzle 1) in Figs. 5 and 6. Figure 5 shows the mean normalized axial velocity profiles (u/U_j) extracted at different downstream locations from the nozzle exit in the major axis plane (subfigure a) and in the minor axis plane (subfigure b). The LES captures the jet behavior observed in the PIV. The jet bifurcates in the major axis just downstream of the centerbody tip and the two potential core regions diverge as the jet spreads. The normalized root mean square (RMS) of the axial velocity (u'/U_j) in the major and minor-planes are presented in Fig. 6. In the major-axis plane, shown in Fig. 6a the four peaks in the RMS values show where the generated shear layers are located and are again an indication of the fact that the

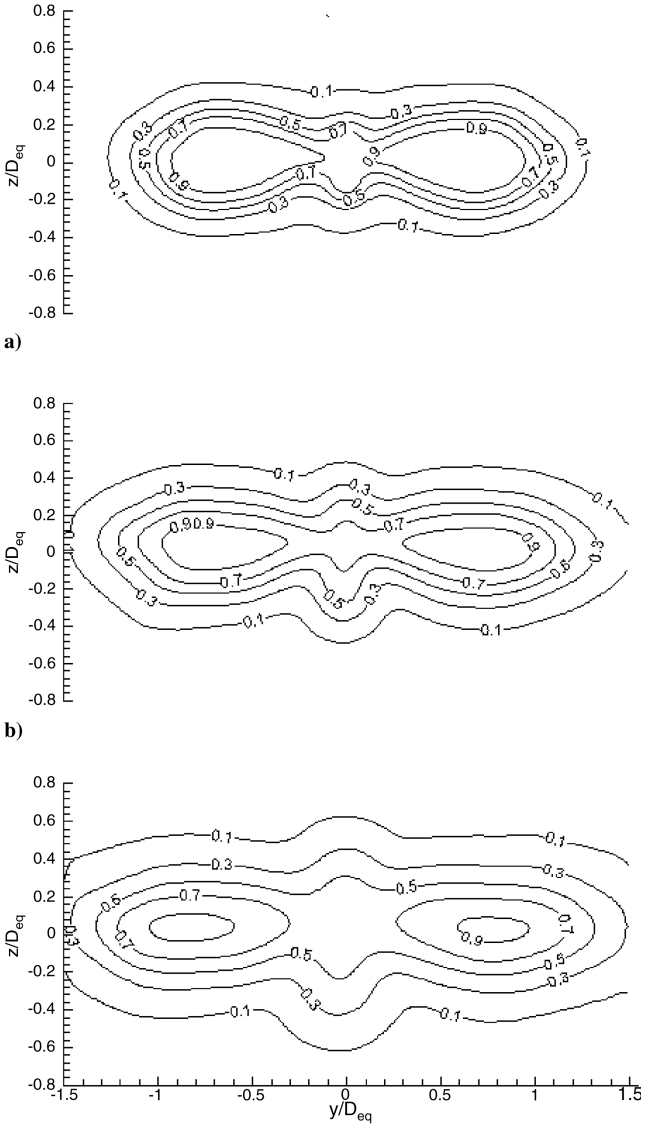

Fig. 3 Normalized mean axial velocity contours (u/U_j) as measured by PIV in planes normal to the nozzle axis at three different locations from the nozzle exit plane, $M_j = 0.96$, $T_0/T_a = 1.26$: a) $x/D_{eq} = 2.27$, b) $x/D_{eq} = 3.23$, and c) $x/D_{eq} = 4.19$.

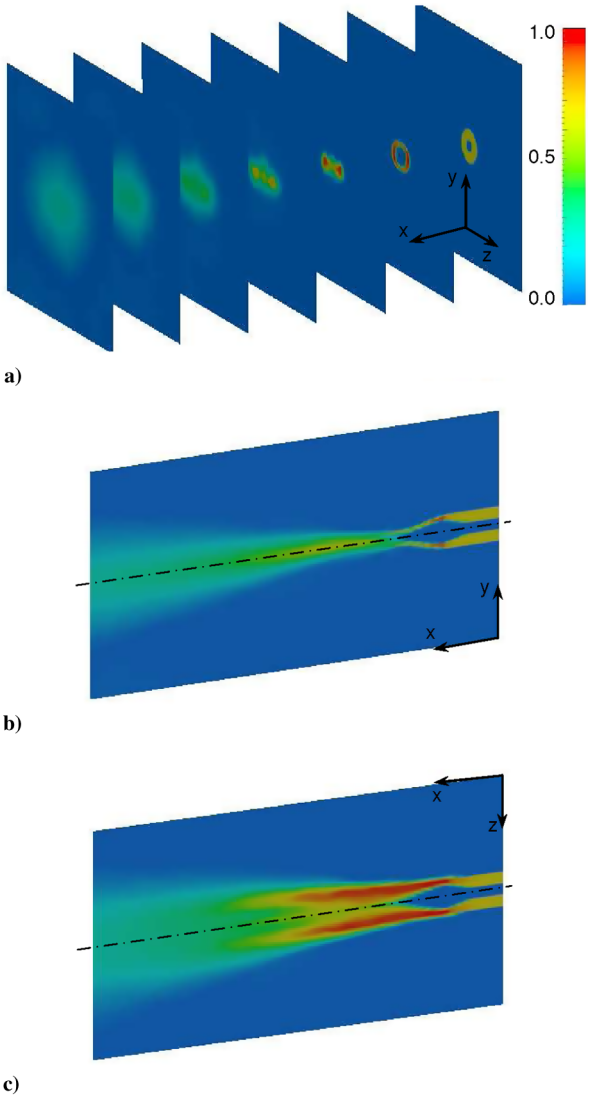

Fig. 4 Normalized time-averaged velocity distributions calculated by LES (nozzle 1): a) cross-sectional planes at different downstream locations from the inlet plane, b) minor-axis plane, and c) major-axis plane.

primary jet splits into two separated jets. In Fig. 6b it is shown that in the minor axis-plane the RMS values of axial velocity present similarities with that of a single stream jet.

Differences between the experimental data and the LES are due to the boundary conditions applied in the calculations at the inlet plane. In the computations a constant (top-hat shape) velocity profile is used, without turbulent fluctuations. In addition, the confinement effects associated with LES may explain why in the experiments the jet spreads faster than in the simulations. This results in a faster decay of turbulence quantities in the downstream region of the jet. The slight asymmetry in the experimental data in the minor axis plane is due to a slight drooping of the centerbody under its own weight.

The fluid flow dynamics and the vortical scales developed in the turbulent flowfield as captured by the LES are depicted in Figs. 7a and 7b. The cores of the vortical structures depicted in Fig. 7a were identified by using the λ_2 vortex visualization method [32], while the vorticity magnitude isocontours shown in Fig. 7b were extracted at several cross-sectional planes downstream of the centerbody tip. Pairs of vortical rings are visible in the major axis plane just downstream of the nozzle. Closer to the nozzle, higher levels of vorticity were found in the shear-layer generated between the high velocity stream and the ambient air, surrounding the bifurcated jet.

Similar vortical rings have been identified by using LES in 4:1 aspect ratio rectangular free jets after an initial axis switch [22,23]. These numerical studies of vortex ring dynamics show that as the bifurcation progresses, global self-deformation may occur and where higher curvature regions of the vortex near the major axis move downstream faster than the lower curvature regions near the minor axis, As a consequence, the major axis portions move toward each other and, the minor axis portions of the vortices move away from each other. This evolution of the rings will eventually lead to the collision of the portions of the vortical rings which were originally near the major axis. Vortex ring bifurcation has been observed experimentally in elliptic jets with aspect ratios above 3.5 but only after the jet initially changed axis [8]. In the present study the jet bifurcation occurs just downstream of the nozzle plug without an initial axis switching, the vortical structures having the same orientation as the elliptic nozzle.

It is customary to track the decay of a jet by tracking the decay of its centerline velocity. Since the potential cores of the bifurcated jets do not follow the nozzle axis, it does not make sense to track the centerline of the nozzle as an indicator of this jet's decay. The velocity that must be tracked instead, U_c, should follow the center of the potential core region. Since the nozzle and the jet are symmetric in the nozzle's major and minor axis planes, and since the bifurcated cores remain in the major axis plane, the location of U_c may be

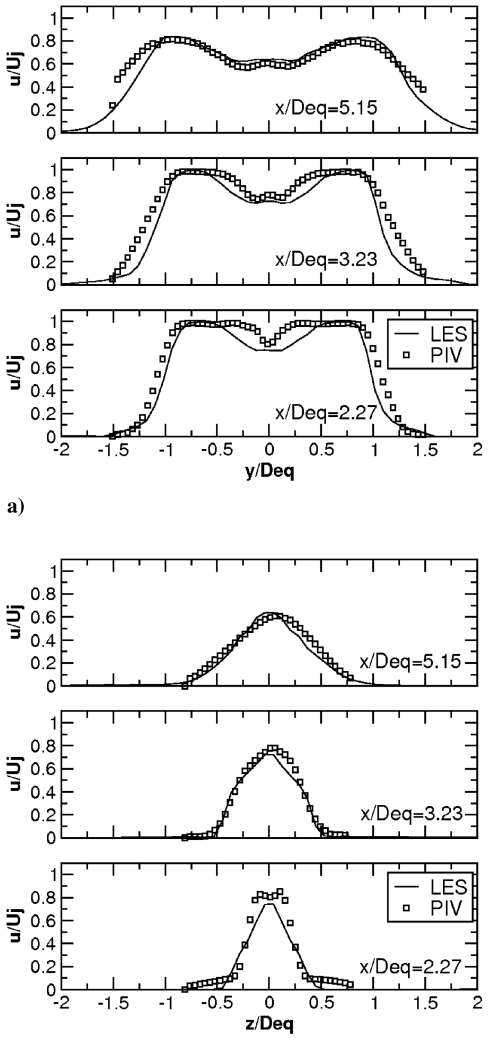

Fig. 5 Normalized mean axial velocity, $M_j = 0.96$, $T_0/T_a = 1.26$: a) major axis plane and b) minor axis plane.

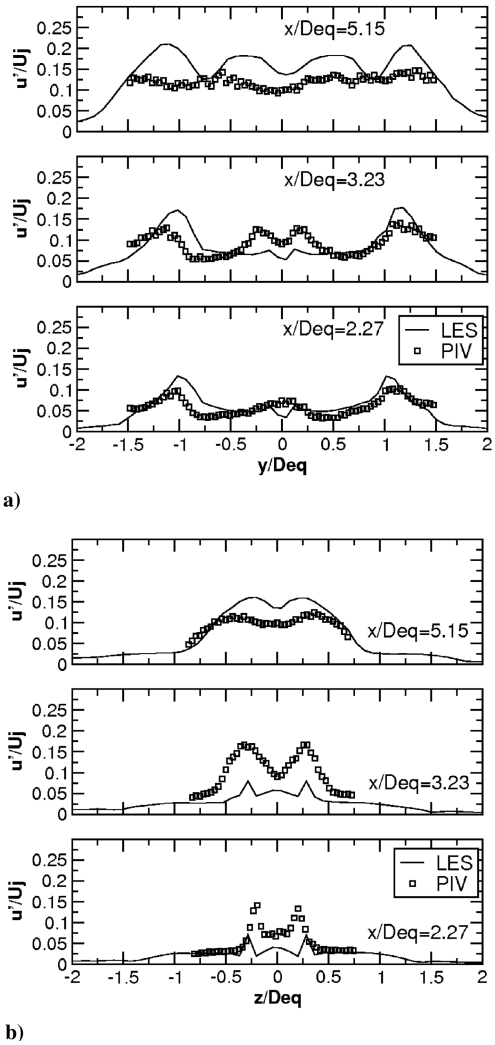

Fig. 6 Normalized RMS of axial velocity. $M_j = 0.96$, $T_0/T_a = 1.26$: a) major axis plane and b) minor axis plane.

identified by a single parameter, y_c, which is a function only of x. More rigorous definitions of U_c and y_c are deferred to Sec. III.B, but let it be noted here, that y_c is a linear function of x, so $y = y_c$ forms a plane, and while there is no symmetry about the plane $y = y_c$ it is in some ways analogous to a minor axis plane for the bifurcated jet.

The decay of U_c is shown in Fig. 8. The agreement between PIV and LES is excellent. Both PIV and LES show no decay in center velocity until past $3.23D_{\text{eq}}$. The experimental data shows velocity decay beginning at $3.7D_{\text{eq}}$, and LES shows that the rate of decay is much higher than the plane elliptic jets reported by Ho and Gutmark [6] or Hussain and Husain [8].

The spreading of the jet in both major axis and minor axis planes is shown in Fig. 9a, and is compared with the 4:1 elliptic nozzle presented by Hussain and Husain [8] which shows a switch of axes at $x/D_{\text{eq}} = 1.95$ before bifurcation and in Fig. 9b is compared with cases where axis switching occurs without bifurcation of the jet. The agreement between PIV and LES is good. The jet spreads and bifurcates without first undergoing a switch of axes.

The entrainment of the jet is plotted in Fig. 10, where Q is the volume flow rate at a given streamwise location, x and Q_0 represents the volume flow rate leaving the nozzle. Thus, $(Q - Q_0)/Q_0$ gives a measure of the entrainment or mixing. Entrainment was integrated over the region plotted in Fig. 3. It can be seen that the entrainment of this jet is similar to that of a round or square jet [6], and a 3:1 ellipse or 3:1 rectangular jet without axis switching [12] but is significantly less than that of a jet undergoing axis switching as Ho and Gutmark's 2:1 elliptic jet did [6].

B. Effects of Mach Number and Temperature

Measurements for a broad range of Mach numbers were taken in a plane normal to the axis at $x/D_{\text{eq}} = 2.03$. Figure 11 depicts the major axis normalized velocity profiles measured at this axial position over a range of Mach numbers from 0.24 to 1.00. There are no significant differences between the profiles at this location for any Mach numbers in the broad range considered.

The development of the jet in the major axis plane as it mixes past the centerbody tip is illustrated in Figs. 12a and 12b for 2 M numbers ($M_j = 0.78$ and $M_j = 0.98$). In both cases the jet was heated ($T_0/T_a = 1.26$). Symbols are shown at every tenth measurement location with solid lines filling in the remaining data points. In these figures the cross-stream distance, y, is nondimensionalized by $y_{0.5}$. The $y_{0.5}$ distance is defined as the y location in the major axis plane where the velocity magnitude U falls to half of U_c, the "center" velocity. The center in this case is not along the nozzle axis, but is rather the centerline of the bifurcated jet. By inspecting Fig. 12 it is found that this center lies at $y_c = 0.6 \bullet y_{0.5}$. This is obviously a circular definition so one must iterate to find $y_{0.5}$, y_c and U_c. The highest velocity observed at a given value of x is taken as an initial estimate of U_c. One can then find $y_{0.5}$ and define $y_c = 0.6 \bullet y_{0.5}$. The next estimate of U_c is then taken as the value of U at $y = y_c$ and $z = 0$. The process is then repeated until successive estimates of U_c have converged to within 0.25 m/s. Similarly $z_{0.5}$ is defined as the value of z at which $U/U_c = 0.5$ in the minor axis and $c_{0.5}$ as the value of z at which $U/U_c = 0.5$, and $y = y_c$. U_c as a function of x/D_{eq} is shown in Fig. 8 and discussed. The evolution of $y_{0.5}$, $y_{0.5}$ and $c_{0.5}$ are shown and discussed next.

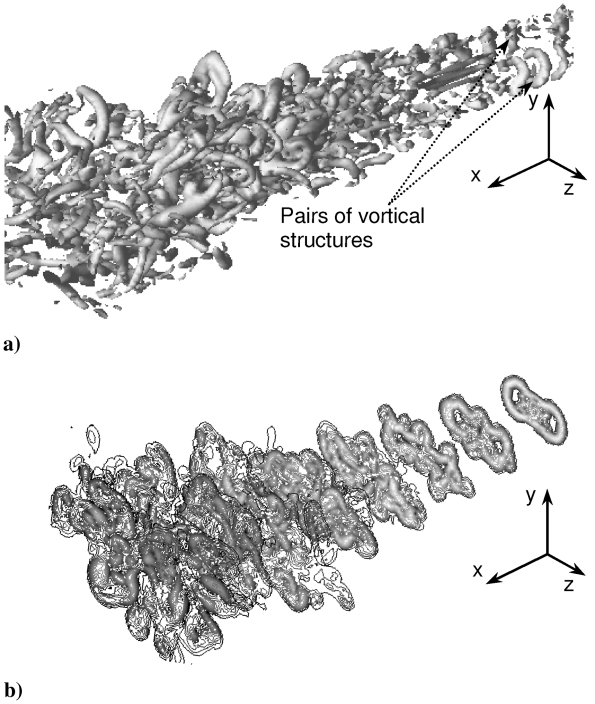

Fig. 7 Snapshots of the structures in the flowfield as captured by LES: a) three-dimensional vortical structures in the flowfield and b) normalized vorticity magnitude isocontours in several cross-sectional planes downstream of the centerbody tip.

Examination of Figs. 12a and 12b shows there is a minimum that develops at $x/D_{\text{eq}} = 2.75$ and $y/y_{0.5} = 0.05$. As the flow further develops it deepens and moves outward, settling at $y/y_{0.5} = 0.13$ by $x/D_{\text{eq}} = 3.71$. As the potential region shrinks it converges to a point $y = y_c$ which lies at $y/y_{0.5} = 0.6$. This is taken to be the center of each bifurcated jet, and the center velocity U_c is taken to be here.

The corresponding velocity profiles in the minor axis plane for the 2 M numbers of $M_j = 0.78$ and 0.96, both heated jets with $T_0/T_a = 1.26$ are shown in Figs. 13a and 13b. Again symbols are only shown for every tenth point with solid lines filling in between. Nearest the centerbody tip at $x/D_{\text{eq}} = 2.27$ the wake of the centerbody generates a minimum at $z/z_{0.5} = 0$. By $x/D_{\text{eq}} = 3.23$ this wake is extinct. Between $x/D_{\text{eq}} = 2.27$ and 3.23 the outer shear layer becomes less steep until by $x/D_{\text{eq}} = 3.23$ is settles into a self-similar shape.

Figure 14 shows the development of the velocity contours in the plane $y = y_c$. This is analogous to a minor axis plane of one of the bifurcated jets. Again 2 M numbers are presented ($M_j = 0.78$ and 0.96), both with $T_0/T_a = 1.26$. Initially there is a significant flat region around $z/z_{0.5} = 0$. By $x/D_{\text{eq}} = 3.23$ the flat region is very small and the contours farther away have settled into a self-similar behavior when scaled by $z_{0.5}$.

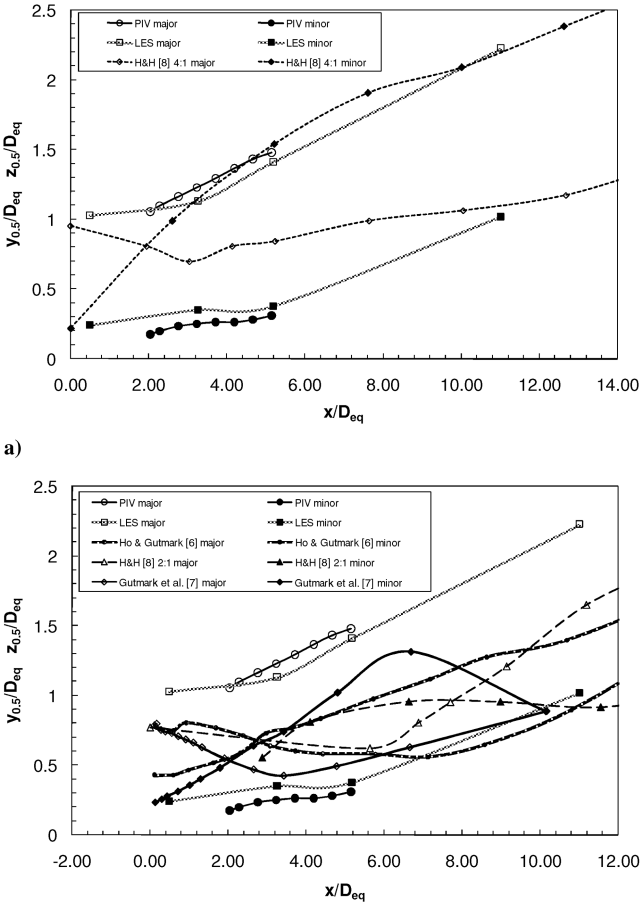

Fig. 9 Jet spreading for $M_j = 0.96$, $T_0/T_a = 1.26$: a) compared with another bifurcating case and b) compared with axis switching cases.

The behavior of the scaling parameters $y_{0.5}$, $z_{0.5}$ and $c_{0.5}$ are shown in Figs. 15a–15c. These parameters are used to track the spread of the jet. The heated jet, with $T_0/T_a = 1.26$ is shown with solid symbols and the unheated jet, $T_0/T_a = 1.0$ is shown with open symbols. Measurements were taken at all streamwise locations for two of the heated cases, $M_j = 0.78$ and $M_j = 0.96$. For these two cases curves are fitted to the data. In subfigure (a) the curves are best-fit lines. In (b) and (c) they are splines fitted through the points.

Figure 15a shows that the overall spreading rate in the major axis plane is linear. It can be seen that at all locations the jet becomes

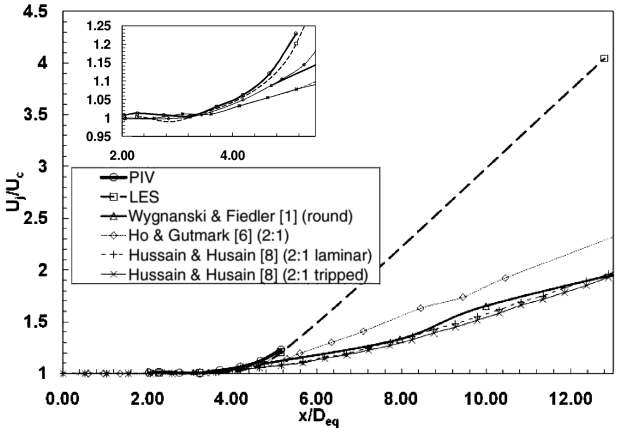

Fig. 8 Decay of U_c the velocity at $x = x_c$ for $M_j = 0.96$, $T_0/T_a = 1.26$ compared with centerline decay for other published cases where $x_c = 0$.

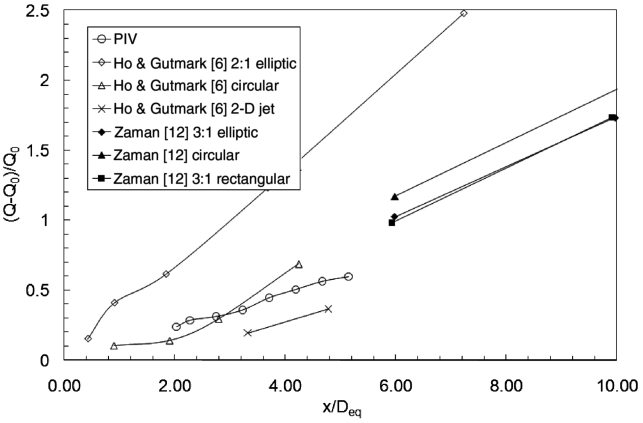

Fig. 10 Entrainment ratio for $M_j = 0.96$, $T_0/T_a = 1.26$ compared with other jets without any centerbody.

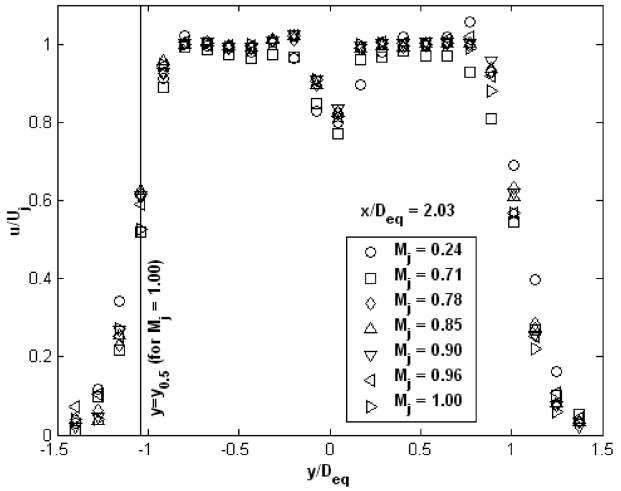

Fig. 11 Normalized mean axial velocity in the major axis for a large range of jet Mach numbers (every 10th point plotted).

narrower as the Mach number is increased and also as the total temperature is increased. For the $M_j = 0.78$ heated case the jet spreads at 7.9° from a virtual origin at $x/D_{\text{eq}} = -5.6$. For the $M_j = 0.96$ heated case the spreading rate is lower at 7.6° and comes

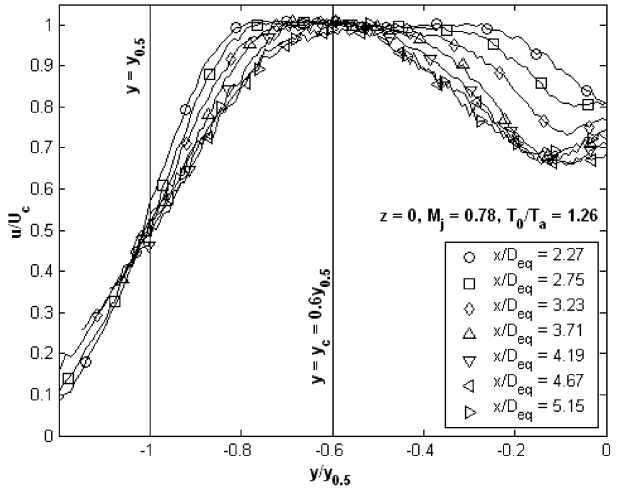

a)

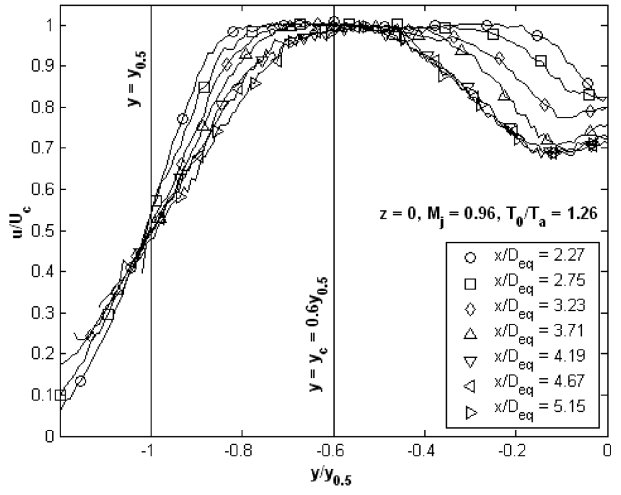

b)

Fig. 12 Normalized mean axial velocity in the major axis as the jet develops downstream: a) $M_j = 0.78$, $T_0/T_a = 1.26$ and b) $M_j = 0.96$, $T_0/T_a = 1.26$.

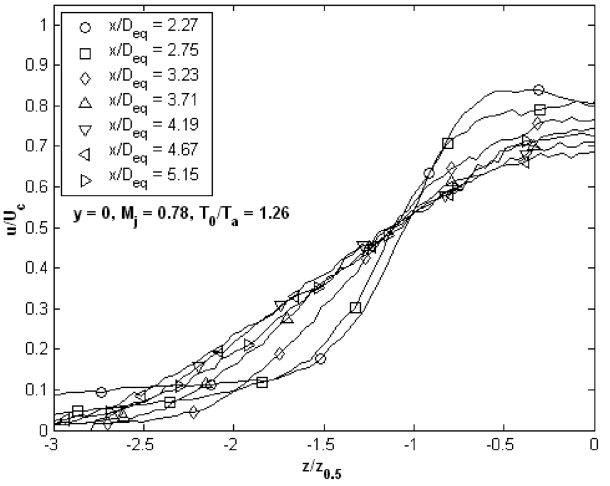

a)

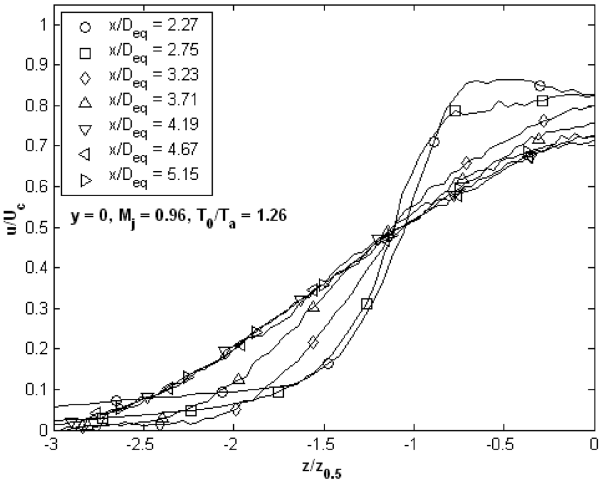

b)

Fig. 13 Normalized mean axial velocity in the minor axis as the jet develops downstream: a) $M_j = 0.78$, $T_0/T_a = 1.26$ and b) $M_j = 0.96$, $T_0/T_a = 1.26$.

from a virtual origin that is farther upstream of the nozzle exit at $x/D_{\text{eq}} = -5.8$.

The spreading in the minor axis plane is shown in Fig. 15b. The overall trend in the minor axis is for the jet to spread. There is an inflexion point in the vicinity of $x/D_{\text{eq}} = 3.8$ where this spreading pauses and then continues. Increasing Mach number causes the jet to become wider in the minor axis, as does increasing the stagnation temperature.

Since the jet has bifurcated it makes sense to look at the spread of each bifurcated jet along the plane $y = y_c$. This plane passes through the center of one of the bifurcated jets, normal to the nozzle major axis. It is analogous to a minor axis of one of the bifurcated jets as it develops. The spread in this plane is tracked by $c_{0.5}$ and is shown in Fig. 15c. The overall trend is for the jet to contract initially, to reach a minimum at around $x/D_{\text{eq}} = 3.8$ and then to begin spreading. There is no uniform trend with Mach number or stagnation temperature. At $x/D_{\text{eq}} = 2.03$ the jet is narrowest at $M_j = 1.00$, broader at $M_j = 0.78$ and broader still at $M_j = 0.96$. At $x/D_{\text{eq}} = 2.27$ and 2.75 all points collapse on one another. At $x/D_{\text{eq}} = 3.23$ all conditions collapse on two points. All the heated conditions and the unheated case at $M_j = 0.96$ have $c_{0.5}/D_{\text{eq}} = 0.241$, while two unheated cases, $M_j = 0.78$ and 1.00 collapse to $c_{0.5}/D_{\text{eq}} = 0.247$. For $x/D_{\text{eq}} = 3.71$, 4.67 and 5.15 the spread is greater for lower Mach number, but for $x/D_{\text{eq}} = 4.19$ all points again collapse, and for $x/D_{\text{eq}} = 4.67$ the $M_j = 1.00$ case collapses upon the $M_j = 0.78$ case giving no monotonic trend.

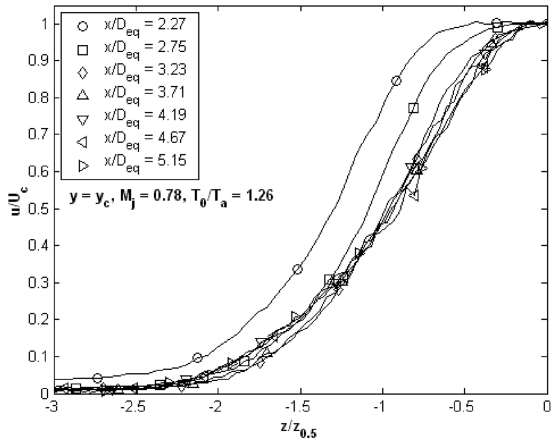

a)

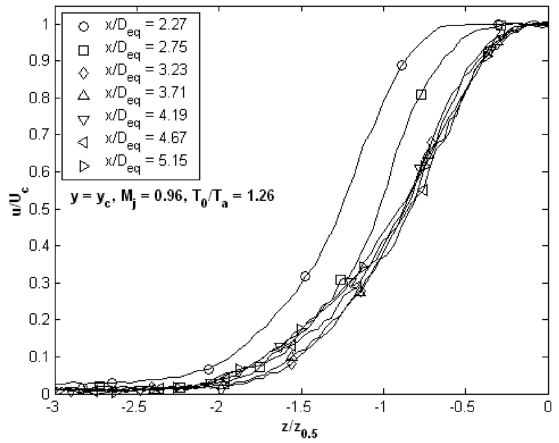

b)

Fig. 14 Normalized mean axial velocity in a plane parallel to the minor axis through $y = y_c$ as the jet develops downstream: a) $M_j = 0.78$, $T_0/T_a = 1.26$ and b) $M_j = 0.96$, $T_0/T_a = 1.26$.

As velocity increases, either because Mach number is increased, or because stagnation temperature raises, increasing the sound speed, the jet consistently spreads less in the major axis and spreads more in the minor. Since both increasing Mach number and increasing total temperature increases the jet velocity it begs the question if this is purely a velocity effect. To examine this question $y_{0.5}/D_{\text{eq}}$ as a function of U_j is plotted in Fig. 16 for the two locations where both hot and cold cases were measured, $x/D_{\text{eq}} = 3.23$ and 4.19. For $x/D_{\text{eq}} = 3.23$ the heated and unheated cases appear to lie on different lines, suggesting that Mach number and total temperature have independent effects on spreading. At $x/D_{\text{eq}} = 4.19$ it is less clear whether heated and unheated cases might align.

C. LES of Alternate Nozzle Configurations

To better understand the bifurcating behavior of the jet from nozzle 1, two additional nozzles (nozzle 2 and nozzle 3) were simulated by LES (see also Fig. 1). Both were analyzed under the heated condition ($T_0/T_a = 1.26$) with a NPR of 1.8, giving a jet Mach number (M_j) of 0.96.

It was originally conjectured that the bifurcation might be caused by the significant inward radial velocity imposed in the minor axis by the inner contour of the nozzle surface. To explore this idea nozzle 2 was generated with the same exit area, but with the negative radial component of velocity reduced so that the flow in the minor axis plane emerges parallel to the centerbody surface.

Hussain and Husain observed bifurcation in plain elliptic jets, but only those with aspect ratios greater than four and only after a single switch of axes [8]. (For lower aspect ratios they observed repeated axis switches.) The behavior of the present jet is different in that it

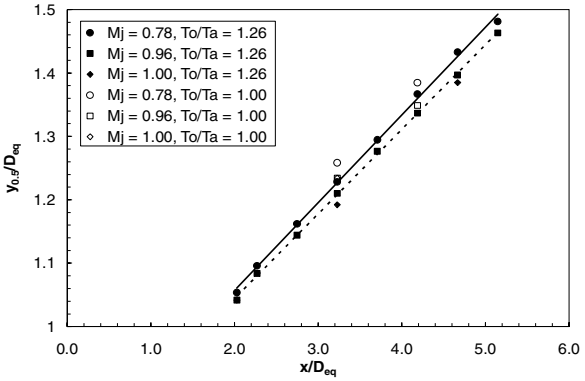

a)

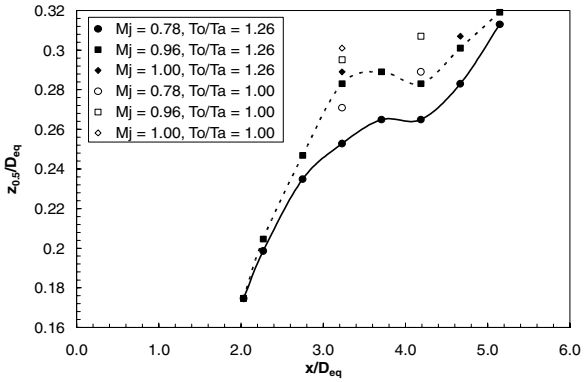

b)

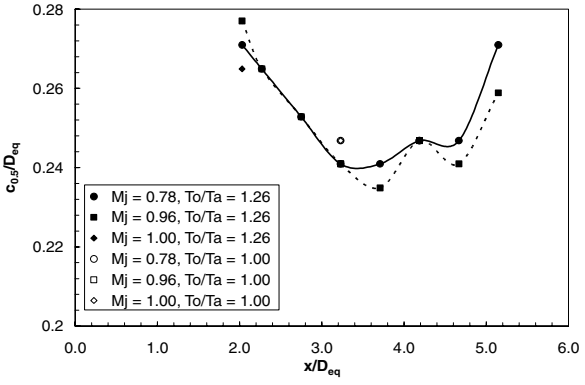

c)

Fig. 15 Jet spreading with axial distance: a) spread of $y_{0.5}$, b) spread of $z_{0.5}$, and c) spread of $c_{0.5}$.

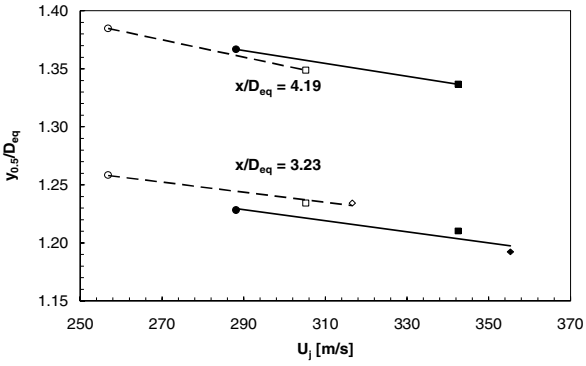

Fig. 16 Major axis width as a function of jet velocity at $x/D_{\text{eq}} = 3.23$ and 4.19; legend as in Fig. 15.

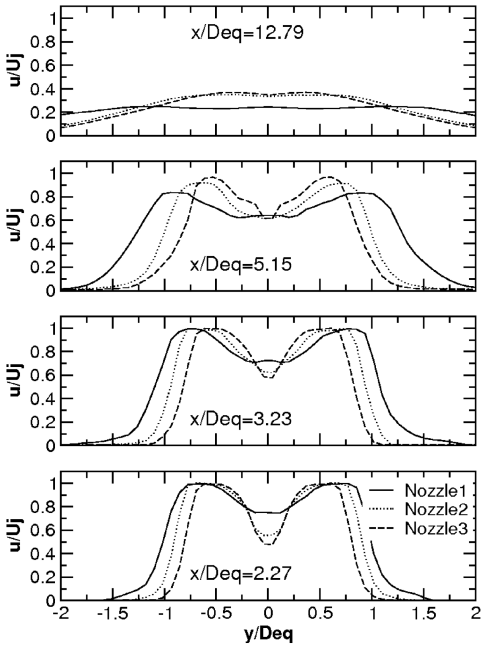

a)

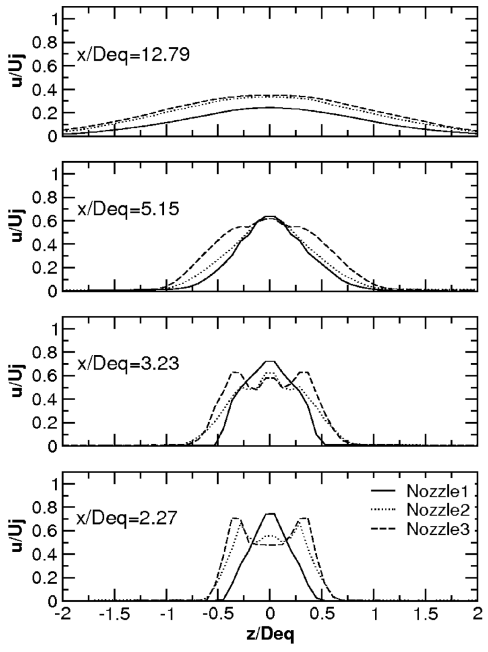

b)

Fig. 17 Normalized time-averaged axial velocity profiles as calculated with LES for nozzle 1, nozzle 2, and nozzle 3 configurations: a) major axis plane and b) minor axis plane.

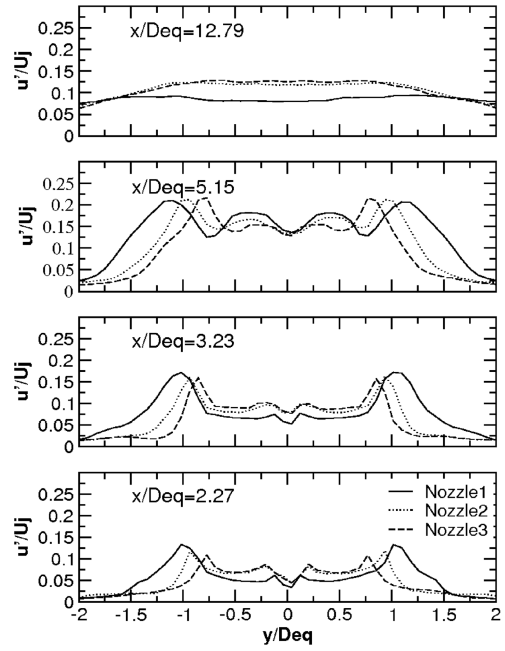

a)

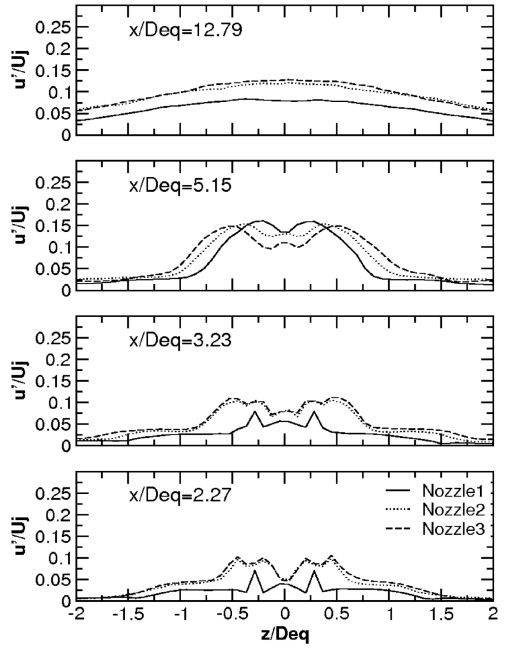

b)

Fig. 18 Normalized RMS values of axial velocity profiles as calculated with LES for nozzle 1, nozzle 2, and nozzle 3 configurations: a) major axis plane and b) minor axis plane.

does not perform an axis switch before bifurcating, but the observations of Hussain and Husain nevertheless suggest that a lower aspect ratio nozzle might not generate a bifurcated jet, so a third 2:1 elliptic nozzle with a round centerbody and without the inward forcing of the flow stream towards the conic plug (nozzle 3) was considered using LES.

Comparisons between the normalized time-averaged axial velocities (u/U_j) calculated by LES are presented for all three elliptic plug nozzles in Figs. 17a and 17b, while the corresponding plots of normalized RMS values of axial velocity (u'/U_j) are depicted in Figs. 18a and 18b. The data were extracted along both major and minor axes at four different positions downstream from the nozzle exit ($2.27D_{eq}$, $3.23D_{eq}$, $5.15D_{eq}$, and $12.79D_{eq}$). It was found

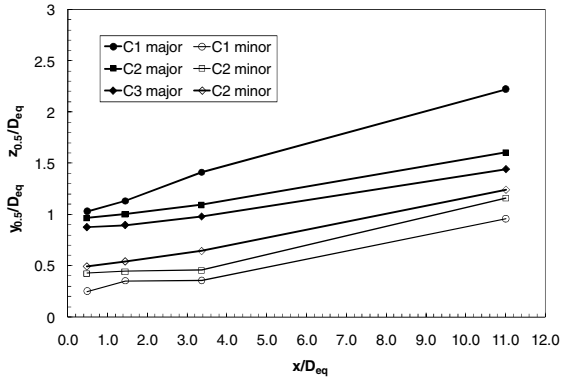

Fig. 19 Jet spread for three nozzle configurations by LES.

that the jet with large negative radial velocity in the minor axis, nozzle 1, spreads the most in the major axis plane and spreads the least in the minor axis plane. Allowing the flow to exit parallel to the plug in the minor axis plane (nozzles 2 and 3) resulted in increased jet spreading in the minor axis and decreased spreading of the jet in the major axis plane as compared with nozzle 1 case.

The spreading of the jet in major and minor axes is shown in Fig. 19. The data show that the axis switching does not occur for any of the configurations analyzed in this study. The nozzle 3 case generated a jet that has the largest spreading in the minor axis plane and the lowest in the major axis plane of all considered geometries.

IV. Conclusions

A plug nozzle with a 3:1 ratio of exit heights might be expected to produce an elliptic jet with a 3:1 aspect ratio. Such a jet might then be expected to undergo axis switching and produce very strong mixing as a result. For aspect ratios below 4:1 Hussain and Husain [8] found axis switching to be the dominant behavior of elliptic jets. Bifurcation is the expected behavior of elliptic jets of aspect ratios above 4:1. So in one sense, it might appear that the introduction of a centerbody had increased the effective aspect ratio of our elliptic jet, but there is more to it than that.

The bifurcation mechanism seen for this jet is clearly different from that observed by Hussain and Husain [8] in that there is no axis switch before the bifurcation. For the 4:1 jet Hussain and Husain observed a single axis switch before bifurcation, and the bifurcated jets spread in their nozzle's minor axis plane. Here it was demonstrated that the present elliptic nozzle with centerbody plug produces no initial axis switch and the jet width in the major axis plane is much greater than the width in the minor axis plane at all locations.

Shortly past the end of the centerbody tip at $x/D_{\text{eq}} = 1.79$ the shear layer from the elliptical nozzle and the boundary layer wake from the centerbody have merged. There is some three-dimensional evolution of the vortex rings as shown in the LES results, but the dominant cause of bifurcation is likely to be the merger of these two shear layers.

One possible mechanism considered was that not only the growth and merger of the inner boundary layer and outer shear layer, but also the driving of the shear layer into the plug by an initial inward component of velocity. LES of the nozzle 2 configuration showed that this was not the cause. Nozzle 2 duplicated most of the conditions of nozzle 1, but altered the inward forcing due to the shape of the nozzle inner contour at the minor axis. The inner contour was reshaped to cause the jet to exit the nozzle without a large inward component of velocity. In this case the jet bifurcated nonetheless.

A second mechanism considered was that the aspect ratio might be high enough to force bifurcation. Nozzle 3 simulated in LES reveals that a substantial reduction in the aspect ratio of the jet alters the degree of spreading in the major axis plane, but that the jet still bifurcates.

The LES calculations supported the experimental measurements and observations in the case of nozzle 1. A fair agreement was found between the LES predictions and the PIV measured data. LES will be further used for investigating different aspect ratios elliptic nozzles and configurations under the same flow conditions.

Acknowledgments

The authors wish to thank General Electric aviation for financial and technical support of this project. They would also like to acknowledge Jeffrey Kastner for providing insightful comments and invaluable feedback regarding this work.

References

[1] Wygnanski, I., and Fiedler, H. E., "Some Measurements in the Self-Preserving Jet," *Journal of Fluid Mechanics*, Vol. 38, No. 3, 1969, pp. 577–612. doi:10.1017/S0022112069000358

[2] Crow, S. C., and Champagne, F. H., "Orderly Structure in Jet Turbulence," *Journal of Fluid Mechanics*, Vol. 48, No. 3, 1971, pp. 547–591. doi:10.1017/S0022112071001745

[3] Hussein, H. J., Capp, S. P., and George, W. K., "Velocity Measurements in a High-Reynolds-Number, Momentum Conserving, Axisymmetric, Turbulent Jet," *Journal of Fluid Mechanics*, Vol. 258, No. -1, 1994, pp. 31–75. doi:10.1017/S002211209400323X

[4] Hussein, H. J., Capp, S. P., and George, W. K., "Round Turbulent Jet," *A Selection of Test Cases for the Validation of Large-Eddy Simulation of Turbulent Flows*, AGARD AR-345, 1998, pp. 154–155.

[5] Krothapalli, A., Baganoff, D., and Karamcheti, K., "On the Mixing of a Rectangular Jet," *Journal of Fluid Mechanics*, Vol. 107, No. -1, 1981, pp. 201–220. doi:10.1017/S0022112081001730

[6] Ho, C-M., and Gutmark, E., "Vortex Induction and Mass Entrainment in a Small-Aspect-Ratio Elliptic Jet," *Journal of Fluid Mechanics*, Vol. 179, No. -1, 1987, pp. 383–405. doi:10.1017/S0022112087001587

[7] Gutmark, E. J., Schadow, K. C., Parr, T. P., Hanson-Par, D. M., and Wilson K. J., "Noncircular Jets in Combustion Systems," *Experiments in Fluids*, Vol. 7, No. 4, 1989, pp. 248–258.

[8] Hussain, F., and Husain, H. S., "Elliptic Jets. Part 1: Characteristics of Unexcited and Excited Jets," *Journal of Fluid Mechanics*, Vol. 208, No. -1, 1989, pp. 257–320. doi:10.1017/S0022112089002843

[9] Reynolds, W. C., Parekh, D. E., Juvet, P. J. D., and Lee, M. J. D., "Bifurcating and Blooming Jets," *Annual Review of Fluid Mechanics*, Vol. 35, No. 1, 2003, pp. 295–315. doi:10.1146/annurev.fluid.35.101101.161128

[10] Husain, H. S., and Hussain A. K. M. F., "Controlled Excitation of Elliptic Jets," *Physics of Fluids*, Vol. 26, No. 10, 1983, pp. 2763–2766. doi:10.1063/1.864062

[11] Toyoda, K., Shirahama, Y., and Kotani, K., "Manipulation of Vortical Structures in Noncircular Jets," *Japan Society of Mechanical Engineers, Transactions B*, Vol. 58, 1992, pp. 7–13.

[12] Zaman, K. B. M. Q., "Spreading Characteristics of Compressible Jets from Nozzles of Various Geometries," *Journal of Fluid Mechanics*, Vol. 383, 1999, pp. 197–228. doi:10.1017/S0022112099003833

[13] Koshigoe, S., Gutmark, E., Schadow, K., and Tubis, A., "Initial Development of Non Circular Jets Leading to Axis Switching," *AIAA Journal*, Vol. 27, No. 4, 1989, pp. 411–419. doi:10.2514/3.10128

[14] Zaman, K. B. M. Q., "Axis Switching and Spreading of an Asymmetric Jet: The Role of Coherent Structure Dynamics," *Journal of Fluid Mechanics*, Vol. 316, No. -1, 1996, pp. 1–27. doi:10.1017/S0022112096000420

[15] Habli, S., Mhiri, H., El Golli, S., Le Palec, G., and Bournot, P., "Numerical Study of Inflow Conditions on an Axisymmetric Turbulent Jet," *International Journal of Thermal Sciences*, Vol. 40, No. 5, 2001, pp. 497–511. doi:10.1016/S1290-0729(01)01238-8

[16] Rembold, B., Adams, N. A., and Kleiser, L., "Direct Numerical Simulation of a Transitional Rectangular Jet," *International Journal of Heat and Fluid Flow*, Vol. 23, No. 5, 2002, pp. 547–553. doi:10.1016/S0142-727X(02)00150-9

[17] Hilgers, A., and Boersma, B. J., "Optimization of Turbulent Jet Mixing," *Fluid Dynamic Research*, Vol. 29, 2001, pp. 345–368.

[18] Miller, R. S., Madina, C. K., and Givi, P., "Numerical Simulation of Noncircular Jets," *Computers and Fluids*, Vol. 24, No. 1, 1995, pp. 1–25. doi:10.1016/0045-7930(94)00019-U

[19] Vreman, B., Geurts, B., and Kuerten, H., "Subgrid-Modeling in LES of Compressible Flow," *Applied Scientific Research*, Vol. 54, No. 3, 1995, pp. 191–203. doi:10.1007/BF00849116

[20] Olsson, M., and Fuchs, L., "Large Eddy Simulation of the Proximal Region of a Spatially Developing Circular Jet," *Physics of Fluids*, Vol. 8, No. 8, 1996, pp. 2125–2137. doi:10.1063/1.868987

[21] Bogey, C., and Bailly, C., "Computation of the Self Similarity Region of a Turbulent Round Jet Using Large-Eddy Simulation," *Proceedings of Direct and Large-Eddy Simulation VI- DLES 6*, 2005.

[22] Grinstein, F. F., "Self-Induced Vortex Ring Dynamics in Subsonic Rectangular Jets," *Physics of Fluids*, Vol. 7, No. 10, 1995, pp. 2519–2521. doi:10.1063/1.868699

[23] Grinstein, F. F., "Vortex Dynamics and Entrainment in Rectangular Free Jets," *Journal of Fluid Mechanics*, Vol. 437, 2001, pp. 69–101.
[24] Paliath, U., and Morris, P. J., "Prediction of Jet Noise from Rectangular Nozzles," AIAA Paper 2006-618, 2006.
[25] Callender, B., Univ. of Cincinnati, Gutmark, E., and Dimicco, R., "The Design and Validation of a Coaxial Nozzle Acoustic Test Facility," 40th AIAA Aerospace Sciences Meeting, Reno, NV, 14–17 Jan. 2002, AIAA Paper 2002-369, 2002.
[26] Rai, M. M., and Moin, P., "Direct Simulations of Turbulent Flow Using Finite-Difference Schemes," *Journal of Computational Physics*, Vol. 1, No. 1, 1991, pp. 15–53.
[27] Gullbrand, J., Bai, X. S., and Fuchs, L., "High-Order Cartesian Grid Method for Calculation of Incompressible Turbulent Flows," *International Journal for Numerical Methods in Fluids*, Vol. 36, No. 6, 2001, pp. 687–709.
doi:10.1002/fld.152
[28] Szasz, R. Z., Revstedt, J., and Fuchs, L., "Comparison of Some SGS Models for Turbulent Fluxes of Momentum and a Passive Scalar in Swirling Co-Annular Jets," *5th IUTAM Symposium on Direct and Large Eddy Simulation V, DLES-5*, edited by R. Friedrich and O. Metais, Kluwer Academic, Norwell, MA, 2004, pp. 545–554.
[29] Mihaescu, M., Szasz, R. Z., Fuchs, L., and Gutmark, E. J., "Coaxial Jet Noise Prediction: Grid Resolution Effect on the Numerical Solution," AIAA Paper 2005-3087, 2005.
[30] Gullbrand, J., Bai, X. S., and Fuchs, L., "Large Eddy Simulation of Turbulent Reacting Flows Using Cartesian Grid and Boundary Corrections," AIAA Paper 1998-3317, 1998.
[31] Mihăescu, M., Harris, C., Gutmark, E. J., and Fuchs, L., "Flow and Acoustics Characteristics of Chevron Nozzles in Coaxial Jets: LES and Acoustic Analogy Investigation," AIAA Paper 2007-3609, 2007.
[32] Joeng, J., and Hussain, F., "On the Identification of a Vortex," *Journal of Fluid Mechanics*, Vol. 285, No. -1, 1995, pp. 69–94.
doi:10.1017/S0022112095000462

L. Cattafesta
Associate Editor